

# Multi-criteria optimization of the spatial dose distribution

Alexander Schlaefer

*Medical Robotics Group, Universität zu Lübeck, Germany and Institute of Medical Technology, Hamburg University of Technology, Germany*

Tiberiu Viulet

*Medical Robotics Group, Universität zu Lübeck, Germany*

Alexander Muacevic

*European CyberKnife Center Munich, Germany*

Christoph Fürweger

*European CyberKnife Center Munich, Germany*

(Dated: November 18, 2013)

Purpose: Treatment planning for radiation therapy involves trade-offs with respect to different clinical goals. Typically, the dose distribution is evaluated based on few statistics and dose-volume histograms. Particularly for stereotactic treatments, the spatial dose distribution represents further criteria, e.g., when considering the gradient between subregions of volumes of interest. We have studied how to consider the spatial dose distribution using a multi-criteria optimization approach.

Methods: We have extended a step-wise multi-criteria optimization approach to include criteria with respect to the local dose distribution. Based on a three-dimensional visualization of the dose we use a software tool allowing interaction with the dose distribution to map objectives with respect to its shape to a constrained optimization problem. Similarly, conflicting criteria are highlighted and the planner decides if and where to relax the shape of the dose distribution.

Results: To demonstrate the potential of spatial multi-criteria optimization, the tool was applied to a prostate and meningioma case. For the prostate case, local sparing of the rectal wall and shaping of a boost volume are achieved through local relaxations and while maintaining the remaining dose distribution. For the meningioma, target coverage is improved by compromising low dose conformality towards non-critical structures. A comparison of dose-volume histograms illustrates the importance of spatial information for achieving the trade-offs.

Conclusion: The results show that it is possible to consider the location of conflicting criteria during treatment planning. Particularly, it is possible to conserve already achieved goals with respect to the dose distribution, to visualize potential trade-offs, and to relax constraints locally. Hence, the proposed approach facilitates a systematic exploration of the optimal shape of the dose distribution.

## I. INTRODUCTION

Radiation therapy treatment planning naturally involves trade-offs, e.g., between coverage of the target with the prescribed dose and sparing of surrounding tissue and critical structures. When inverse plan optimization is employed, the various clinical goals are expressed by mathematical terms included in the objective function of an optimization problem. One approach to find a trade-off among the conflicting goals is to allow for user-defined weighting factors reflecting the relative importance of each term<sup>1-3</sup>. However, re-iterating through the optimization for different importance factor settings can be cumbersome and time consuming. Moreover, it is often not clear whether the current solution can be improved further. This motivates approaching planning as a multi-criteria problem where Pareto-efficient solutions are identified<sup>4-8</sup>. By definition these solutions cannot be improved with respect to any one clinical goal without sacrificing at least one other clinical goal. Clearly, the optimal solution of the planning problem will be Pareto-efficient. Hence, planning is reduced to finding the particular Pareto-efficient solution that represents the most desirable trade-off to the hu-

man planner.

Different methods can be employed to facilitate this search. One option is to initially approximate the Pareto-frontier and to generate a database with Pareto-efficient solutions representing different preferences with respect to the different goals. The human planner can then navigate through the database and select the most desirable trade-off<sup>9-12</sup>. Clearly, storing solutions for small variations with respect to the preference of the criteria leads to a large database. In practice a coarser approximation of the Pareto-frontier may be used, where intermediate solutions are interpolated during navigation. However, the search space still grows exponentially with the number of criteria that is considered, which usually include basic dose statistics like minimum, mean, or maximum dose in the different volumes of interest (VOIs).

Another method is approaching the search by a sequence of optimization steps with respect to different planning criteria. Hard constraints are imposed on all but one criteria, i.e., the plan quality with respect to these criteria cannot degrade. The remaining criterion forms the objective function. If a sequence of optimization steps is preformed this results in a pri-

oritization of the first criterion over subsequent criteria<sup>13,14,115</sup>. However, optimization steps can also be run interactively and in any order, leading to step-wise multi-criteria optimization (SMCO)<sup>15,16</sup>. After each optimization step, the best solution with respect to the chosen objective is obtained. Any further improvement requires relaxing at least one of the constraints,<sup>120</sup> i.e., the human planner decides what trade-off would be desirable. When ultimately optimization steps with respect to all criteria have been performed, a Pareto-optimal solution has been found. This approach requires the optimization to be fast and, for a large number of steps, can take substantial time<sup>125</sup> to complete.

In practice, an experienced human planner will often start with dose bounds that lead to a reasonable first plan. Moreover, after each step the planner gains information on the feasible solutions. Hence, the step-wise exploration of potential<sup>130</sup> trade-offs will be more directed and cover a smaller subset of the Pareto-frontier in the proximity of the initial solution. Furthermore, the method may be more suitable to consider complex criteria. We have previously proposed to include the spatial dose-distribution, which can be a key criteria for<sup>135</sup> stereotactic treatments with high doses and steep gradients towards critical structures<sup>17-19</sup>. For example, with the advent of improved functional imaging, 'dose painting' approaches taking into account tumor foci or nerves have been studied more intensely<sup>20-25</sup>. Extending this idea we show how the step-wise<sup>140</sup> optimization framework can be used to achieve multi-criteria control over the spatial dose distribution. First, we present the underlying optimization model. Second, the rationale for spatial trade-offs is motivated. Third, we describe our implementation of a tool facilitating multi-criteria planning of<sup>145</sup> the three-dimensional dose distribution. Finally, we illustrate how the method can be used to optimize the spatial trade-off for exemplary clinical cases.

## II. METHODS AND MATERIAL

### II.A. The optimization framework

We first show how the SMCO framework extends to criteria on the spatial dose distribution. As the basis for plan<sup>110</sup> optimization we adopt the model presented in<sup>16</sup>, i.e., we solve a linear programming optimization problem of the following form

$$\begin{aligned}
 \min \quad & c_x^T x + c_s^T \hat{s} + c_{\check{s}}^T \check{s} + c_{\hat{t}}^T \hat{t} + c_{\check{t}}^T \check{t} \\
 \text{s.t.} \quad & Ax - \hat{s} \qquad \qquad -\hat{t} \leq b_u \\
 & Ax \qquad \qquad +\check{s} \qquad \qquad +\check{t} \geq b_l \\
 & x \leq b_w \\
 & \hat{s} \leq b_{\hat{s}} \\
 & \check{s} \leq b_{\check{s}} \\
 & \hat{t} \leq b_{\hat{t}} \\
 & \check{t} \leq b_{\check{t}} \\
 & \mathbf{1}^T x \leq b_d \\
 & M\hat{s} \leq b_{\hat{a}} \\
 & M\check{s} \leq b_{\check{a}} \\
 & x, \hat{s}, \check{s}, \hat{t}, \check{t} \geq \mathbf{0}
 \end{aligned}$$

where the matrix  $A$  contains the dose deposition coefficients for each beam and voxel,  $x$  is a vector containing the non-negative beam weights,  $c_x$  contains the objective function coefficients for the beams,  $b_u$  and  $b_l$  contain the upper and lower dose bounds for each voxel, and  $b_w$  is the maximum weight per beam. Moreover, the additional slack variables  $\hat{s}$ ,  $\check{s}$  control the deviation from the desired bounds per voxel and  $\hat{t}$ ,  $\check{t}$  control the deviation from the desired bounds per VOI, i.e., the latter have as many components as there are VOIs. The values the slack variables can take are bounded by  $b_{\hat{s}}$ ,  $b_{\check{s}}$ ,  $b_{\hat{t}}$ , and  $b_{\check{t}}$ , and their objective function coefficients are denoted by  $c_{\hat{s}}$ ,  $c_{\check{s}}$ ,  $c_{\hat{t}}$ , and  $c_{\check{t}}$ . The term  $\mathbf{1}^T x$  yields the total monitor units (MU), which is bounded by  $b_d$ . The matrix  $M$  denotes a mapping from voxels to VOI such that the mean deviation from lower and upper bounds per VOI can be maintained by  $b_{\hat{a}}$  and  $b_{\check{a}}$ , respectively.

Given that the objective function is linear, it is easy to see that the number of voxels per VOI will lead to an implicit weighting of the related objective terms. Moreover, the dose delivered to a voxel does not change linearly, e.g., with its distance to a beams's centerline. This is represented in the dose deposition coefficient matrix. As illustrated in<sup>16</sup>, finding objective coefficients that realize a desired trade-off among conflicting criteria is therefore not straightforward. Hence, a key idea of the step-wise approach is to set the objective coefficients in a way that avoids optimization with respect to two criteria at the same time. All objective function coefficients are set to 0, except for those related to the single criterion that is optimized. The plan quality with respect to all remaining criteria is maintained by the hard constraints introduced in the linear program. Relaxing these constraints can result in an improved objective value, and a sequence of optimization and relaxation steps can be performed to search for a Pareto-optimal solution. For example, after specifying reasonable bounds on all organs at risk (OARs) a first step would be to optimize for planning target volume (PTV) coverage. If the resulting coverage is not satisfactory, the planner knows that a further relaxation of at least one OAR bound will be required to increase it further. Otherwise, if coverage is good, it can be turned into a bound and other criteria like further OAR sparing or reduction of the total MU may be considered in a next optimization step. Finally, all optimization steps should be repeated without any relaxation to establish Pareto-efficiency.

The solution resulting from this step-wise approach is Pareto-optimal with respect to the planning criteria considered during the search, which are typically defined based on the VOI. Examples include the minimum, mean, or maximum dose for the PTV, the maximum or mean dose for OARs, and the coverage and conformality of the dose distribution with respect to the PTV. Optimization regarding these criteria is straightforward, as it simply requires setting the objective function coefficients for voxels of the VOI under consideration to 1, and all others to 0.

### II.B. Controlling the spatial dose distribution

Clearly, choosing the VOI as the level of abstraction is somewhat arbitrary. The key idea of inverse planning is to

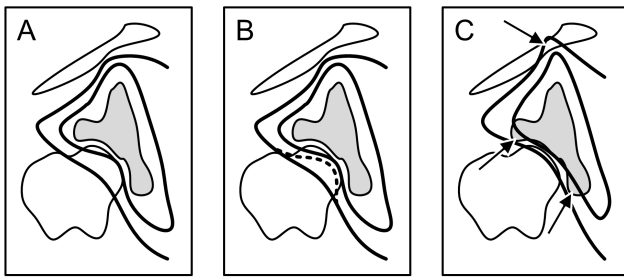


Figure 1 An illustration of a trade-off represented by iso-doses. (a) The scenario includes the PTV (gray), two OAR (white), and the two bold iso-dose lines representing the lower PTV bound and the upper OAR bound, respectively. (b) It would be preferable to modify the iso-dose to the dotted shape, which requires relaxation of bounds. (c) A possible result of relaxation with dose-volume constraints. Arrows indicate problematic regions.

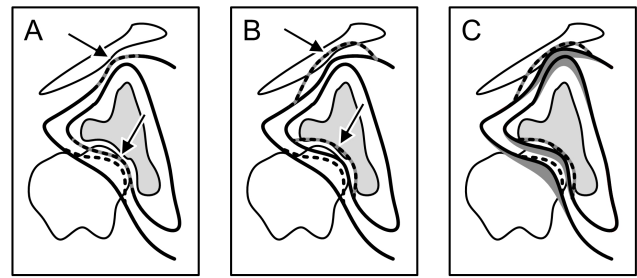


Figure 2 Continuing the example from Figure 1 to illustrate local relaxation. (a) The actually limiting regions on the iso-dose are highlighted. (b) Graphical visualization of a reasonable relaxation of the iso-dose shape. (c) A subsequent optimization could move the iso-doses as indicated by the dark gray regions, the desired improvement can be realized only partially, as the constraints limit further progress. The trade-off becomes obvious.

compute treatment parameters that fulfill a set of criteria with respect to the dose distribution. This distribution may be inhomogeneous and adapted, e.g., to consider information on the expected location of the tumor. Recent advances in functional imaging and the ability of treatment systems to facilitate precise intensity modulated dose delivery have led to substantial interest in dose painting approaches. However, just like inverse planning cannot always fulfill all criteria with respect to the different VOI, it also cannot produce every 'painted' dose distribution. In fact, the conflicting nature of planning again motivates the search for a solution that represents the best trade-off.

Particularly, understanding the conflict between different parts of the dose distribution may be hard. Consider the scenario shown in Figure 1a where the gray region denotes the PTV, the two white regions above and to the left denote OARs, and the two bold lines represent two iso-doses. If the outer iso-dose corresponds to the maximum dose bound for the OAR it would be preferable to improve the sparing of the OAR by moving the iso-dose towards the dotted line shown in Figure 1b. Typically this will not be possible without relaxing some other constraints. One obvious approach would be to relax the minimum dose of the PTV and the maximum dose for the other OAR. To avoid huge changes to the overall dose distribution, a dose-volume constraint (DVC) may be added, i.e., the percentage of the volume subjected to a dose deviating from the previous bound is limited. Interestingly, this would still allow for a poor solution as illustrated in Figure 1c, where the conformality is compromised and the critical iso-dose is cutting through the OAR, as denoted by the arrows.

While changing the DVC may improve the result slightly, there remains a fundamental limitation in this approach. The dose-volume histogram (DVH) does not contain information on the spatial location of the regions that are close to the respective dose bounds. Likewise, the DVC does not allow for control over where the voxels exceeding the dose bound are inside the VOI. This is not intuitive for the planner, who may have a very clear perception where there is room for compromise. Consider Figure 2a, which shows the same scenario. Again, the goal is to move the outer iso-dose towards the dot-

ted line. However, now the regions where constraints on the iso-dose limit the optimization are illustrated (gray and black dotted parts of the iso-dose lines, as indicated by the arrows). Continuing the graphical example, we could now relax the dose bounds by setting the desired iso-doses as shown in Figure 2b, where the areas highlighted by arrows would still represent an acceptable dose distribution. A further attempt at the initial optimization leads to the result presented in Figure 2c, where the dark gray regions denote how much the iso-doses have changed. Clearly, we expect the improvement to be smaller than for the scenario in Figure 1c. In fact, the change of the iso-dose lines after relaxation shows the trade-off among the planning goals. We could continue to relax and optimize to explore what other trade-offs are possible, but at some point we would conclude that one solution represents the optimal balance with respect to our clinical goals. Note that this would not take many iterations, because the constraints that limit progress and are thus candidates for relaxation would be highlighted.

## II.C. Implementation of spatial multi-criteria optimization

The typical approach to planning is to contour the patient anatomy on axial CT-slices and to further discretize the different structures into sets of voxels. Considering that each voxel is represented by a constraint in the optimization problem the vector of dose values can be computed as  $d = Ax$ , i.e., the  $d_i$  is the dose for the  $i$ -th voxel  $v_i$ . These values can be readily obtained from the solver after each optimization step. Moreover, it is straightforward to compute the dose for points outside the contoured volumes of interest by summing the dose deposited by all beams. Based on the voxel doses we can compute and display three-dimensional iso-dose surfaces.

In the step-wise optimization framework we have two types of interactions at the optimization level: setting the optimization goal and relaxing constraints. When interacting with the spatial dose distribution, there are two main scenarios, namely that a set of voxels needs to be inside an iso-dose-surface and that a set of voxels needs to be outside an iso-dose surface. Ei-

ther goal can be expressed by an objective function containing  
 250 only the voxels under consideration. Progress with respect to  
 the objective will be limited by bounds on the dose elsewhere  
 defined by our hard constraints. To illustrate how close an  
 iso-dose surface is to a bound, we use a color scheme where  
 red indicates no slack and blue indicates large slack. Decreasing  
 255 the bound for lower bound constraints and increasing the  
 bound for upper bound constraints adds additional slack and  
 hence allows the iso-dose to move in the desired direction.  
 Before a new goal is considered, the bounds of the constraints  
 are updated to maintain the current dose distribution.

### 260 II.C.1. Goal selection

Consider a set of voxels  $V$  and a threshold  $k$  such that  $V$   
 contains all voxels with a dose larger than or equal to  $k$ . The  
 3D surface covering  $V$  is the  $k$ -iso-dose surface. Let  $G$  be the  
 the set of voxels that should be covered by the  $k$ -iso-dose. If  
 265 the clinical goal is to cover an additional region with the  $k$ -iso-  
 dose, the planner will graphically pull the respective surface  
 in the desired direction. Now let  $i$  run over the indicies of  
 all voxels in  $G \setminus V$ . Then the lower bound  $b_{\tilde{s}_i}$  on each cor-  
 responding lower bound slack variable  $\tilde{s}_i$  is set to the differ-  
 270 ence between the target dose and the current voxel dose, i.e.,  
 $b_{\tilde{s}_i} = k - d_i$ . This allows setting the lower bounds for these  
 voxels to the target dose  $b_{l_i} = k$  and prevents each voxel's  
 dose from decreasing. Finally, we set the goal of the opti-  
 mization as the minimization of the sum of the slack variables  
 275 by setting  $c_{\tilde{s}_i} = 1$  only for the respective voxels. Constraints  
 corresponding to all other clinical criteria remain fixed, result-  
 ing in the simplified linear program

$$\begin{aligned}
 \min \quad & \sum_i c_{\tilde{s}_i} \tilde{s}_i \\
 \text{s.t.} \quad & Ax \leq b_u \\
 & Ax + \tilde{s} \geq b_l \\
 & x \leq b_w \\
 & \tilde{s}_i \leq b_{\tilde{s}_i} \\
 & x, \tilde{s} \geq \mathbf{0}
 \end{aligned}
 \tag{320}$$

where the remaining slack variables and objective coeffi-  
 cients are 0, and  $b_{\tilde{a}}$  and  $b_{\tilde{a}}$  are set to a very large, non binding  
 280 value. All other bounds remain fixed and the objective is to  
 minimize the deviation from the target dose  $k$  over all voxels  
 in  $G \setminus V$ . We will call this a *selective coverage* (SCO) step.

In a similar fashion it is possible to push the iso-dose away  
 from an area, e.g., to spare a structure. Again, the planner  
 285 starts looking at the iso-dose surface for the respective target  
 dose  $k$  and then pushes the dose in the desired direction. We  
 are now adapting the upper bound slack variables and we let  
 $i$  run over the indicies of all voxels in  $V \setminus G$ . First, the upper  
 bound  $b_{\hat{s}_i}$  on each corresponding upper bound slack variable  
 290  $\hat{s}_i$  is set to the difference between the current dose and the  
 target dose, i.e.,  $b_{\hat{s}_i} = d_i - k$ . Second, the upper bounds  
 for these voxels is set to the target dose  $b_{u_i} = k$ , such that  
 each voxel's dose cannot increase. Finally, only the objective  
 coefficients  $c_{\hat{s}_i}$  are set to 1, leading to the following simplified  
 295 linear program

$$\begin{aligned}
 \min \quad & \sum_i c_{\hat{s}_i} \hat{s}_i \\
 \text{s.t.} \quad & Ax - \hat{s} \leq b_u \\
 & Ax \geq b_l \\
 & x \leq b_w \\
 & \hat{s}_i \leq b_{\hat{s}_i} \\
 & x, \hat{s} \geq \mathbf{0}
 \end{aligned}$$

where the deviation from the upper bound is minimized for  
 $V \setminus G$ , the remaining slack variables and objective coefficients  
 are 0, and  $b_{\tilde{a}}$  and  $b_{\tilde{a}}$  are set to a very large, non binding value.  
 This step will be called *selective sparing* (SSP).

Note that for either step feasibility of the optimization prob-  
 lem is maintained. Moreover, all other constraints including  
 the bound on the total beam weight remain unchanged. To  
 preserve the shape of the  $k$ -iso-dose under consideration, the  
 bounds  $b_u$  and  $b_l$  are updated when another goal is selected.

### II.C.2. Constraint relaxation

The optimization steps are only meaningful if all other con-  
 straints remain fixed and the trade-off among the planning cri-  
 teria becomes obvious, i.e., progress with respect to the se-  
 lected goal will be limited. Generally, we have to consider  
 two different types of constraints controlling the dose distri-  
 bution, namely upper and lower dose bounds. On a more ab-  
 stract level relaxation means that the planner wants to allow  
 more dose in a region where the goal is to maintain a maxi-  
 mum dose, or less dose in a region where the goal is to main-  
 tain a minimum dose. This corresponds to shifting a lower  
 iso-dose surface towards the PTV or a higher iso-dose surface  
 towards a VOI, compare the example in Figure 2. Before we  
 consider these two cases in more detail, we note that we can  
 get the upper and lower dose bounds for each voxel from the  
 constraints defined in our optimization problem. Similarly to  
 the iso-dose surfaces we can also show a three-dimensional  
 surface encompassing a region with a certain value for the  
 bounds. Consider a set of voxels  $L$  and a threshold  $k$  such that  
 $L$  contains all voxels with a lower bound less than or equal to  
 $k$ . Then the 3D surface covering  $L$  is the  $k$ -lower-bound sur-  
 face. Likewise, the  $k$ -upper-bound surface is the 3D surface  
 covering the set  $U$  of all voxels with an upper bound larger  
 than or equal to  $k$ . To further highlight where the related con-  
 straints are binding we set the color of the 3D surfaces to the  
 difference between the dose and the dose bound for voxels on  
 the surface, e.g., blue for a large difference and red for zero  
 difference.

We first consider the case where the planner intends to relax  
 the lower bound on the PTV, e.g. to allow some region of the  
 PTV to have a dose below the desired prescription dose. Let  
 $p$  be the dose considered by the planner. Then the  $p$ -lower-  
 bound surface illustrates constraints preventing the  $p$ -iso-dose  
 surface from moving into the PTV. Now the planner considers  
 where to relax the constraints by studying the  $p$ -lower-bound  
 surface and pushing it towards the PTV. Let  $V$  and  $R$  be the  
 sets of voxels covered by the  $p$ -lower-bound surface before  
 and after relaxation, respectively. Then we then need to adjust  
 the lower bound  $b'_{l_i} = b_{l_i} - \rho$  with  $i$  running over all vox-  
 els in  $V \setminus R$  and  $b'_{l_i}$  and  $\rho$  the new bound and a parameter

345 defining the amount of relaxation, respectively. The case for  
the relaxation of an upper bound on a VOI is similar, i.e., the  
p-upper-bound surface is pushed towards the VOI and the up-  
date of the bounds is  $b'_{u_i} = b_{u_i} + \rho$ . Note that if we assume  
350 that the planner considers iso-dose-surfaces running close to  
the VOI, the iso-dose and bound surfaces will typically almost  
fall together in the region of interest.

Clearly, multiple relaxations do not impair feasibility and  
subsequent re-optimizations with respect to the active goal are  
typically fast. The resulting new dose-distribution will only  
355 change within the defined bounds, i.e., primarily in areas se-  
lected for goal and relaxation. Note that changes in other re-  
gions are only possible within the specified bounds, e.g., the  
dose for an OAR may decrease further.

## II.D. Planning workflow and interaction

360 Based on the outlined goal selection and constraint relax-  
ation the planner can use the tool to explore spatial trade-offs.  
Particularly, the planner gains information on where the con-  
straints are binding, i.e., the dose distribution is not changing  
365 unless the planner explicitly relaxes some constraints. Relax-  
ation will not always result in an improvement with respect  
to the selected goal, e.g., because of other constraints still in  
place. However, once the planner has relaxed the dose con-  
straints in all regions considered potential trade-offs the tool  
370 will readily show the remaining constraints. If these cannot be  
compromised, no further improvement can be expected and  
planning ends, resulting in the following procedure.

1. Decide, whether an area exists where a change in the  
dose would correspond to an improvement in the plan  
and that has not been considered for optimization with  
375 the current bounds  
If yes, select the area and continue  
Else, stop searching and use the current plan
2. Optimize (SCO or SSP step)
3. Study where the dose constraints are binding
- 380 4. Decide, whether some of these constraints can be re-  
laxed  
If yes, relax and go to (2)  
Else, go to (1)

385 Of course, the decision what constitutes a preferable plan  
is upon the planner and there may be different spatial dose  
distributions representing different trade-offs that have simi-  
lar value. Note that the planner could backtrack and explore  
other solutions by applying SCO, SSP, and relaxation. Fur-  
thermore, note that the first step implies that it is necessary  
390 to run all objectives without relaxation to finally establish  
Pareto-efficiency in a lexicographic manner.

In our current implementation the interaction with iso-dose  
or bound surfaces is realized by rotating a 3D scene showing  
the respective 3D surface. The surface is then shaped using  
395 a spherical 'bumper' controlled by the mouse, i.e., the mouse  
motion moves the sphere along the surface and pressing a but-  
ton locally deforms the surface along the sphere.

## II.E. Test data

To demonstrate the potential use of our spatial multi-criteria  
planning approach we selected two clinical cases. First, a  
prostate case was chosen as scenario 1, mainly because it is  
a prominent clinical scenario and rectum and bladder present  
two OARs in direct proximity and to opposite sides of the  
PTV. The main goal was balancing sparing of the rectum  
against PTV coverage and bladder sparing. For the PTV, we  
considered dose criteria proposed for stereotactic body radi-  
ation therapy<sup>26</sup>. Initially, we set a lower bound of 36.25 Gy  
for the PTV and upper bounds of 41.5, 37.0, and 33.0 Gy for  
PTV, rectum, and bladder, respectively. Conformality was en-  
410 forced through the use of two shell structures at 5 mm (36.0  
Gy) and 20 mm (20.0 Gy) distance, and the upper bound on  
the total monitor units (MU) was set to 50000. After optimiz-  
ing for coverage we established whether sparing of the rectal  
wall can be improved by relaxing the constraints in certain  
regions of PTV and bladder. Additionally, we investigated  
whether shaping a high dose boost region inside the prostate  
was feasible with our approach.

Second, a we studied a case with meningioma close to the  
optic nerves and the brainstem and treated with single-session  
radiosurgery. Scenario 2 started from an initial solution with  
good OAR sparing maintained by a 7.0 Gy upper bound, but  
relatively poor PTV coverage at 88.7 % for the prescribed  
dose of 18 Gy (70 % iso-dose). Conformality was maintained  
by shell structures at 5 mm (10 Gy) and 12 mm (4 Gy) dis-  
tance. The goal was to trade-off conformality and OAR spar-  
ing against better PTV coverage.

The optimization problems were set up with a VOI de-  
pendent discretization, and an additional coarse grid to rep-  
resent the dose distribution for interaction. For scenario 1,  
the PTV and coarse interaction grids had an isotropic width  
of 3 mm, for scenario 2 their isotropic width was 1.58  
mm. We adopted the CyberKnife beam delivery model with  
a set of non-coplanar and non-isocentric circular beams start-  
ing at approximately 100 different positions around the pa-  
tient. For both scenarios approximately 1600 candidate beams  
were heuristically generated<sup>27</sup>. Planning results in a subset  
of beams having non-zero weight, e.g., ranging between 283  
and 337 in the subsequent examples. These beams are inde-  
pendently delivered by a robotically positioned beam source.  
Note that the optimization will generally result in a large num-  
ber of candidate beams having zero weight, as minimizing the  
objective function implies that the most effective set of beams  
fulfilling the constraints is chosen. This is particularly clear  
when minimizing the total monitor units. All planning was  
done with our inhouse planning environment using the Cplex  
solver 12.1 (IBM) on a computer with an Core i7 970 CPU  
and 24 GB of RAM running Linux.

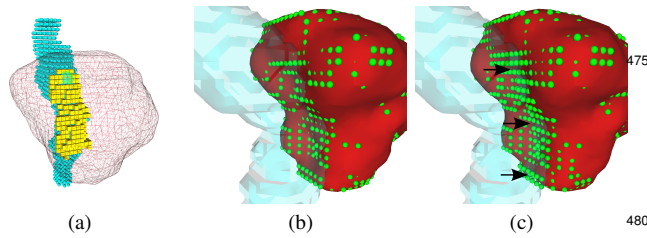


Figure 3 (a) The subset of voxels of the rectum selected as target (cubes) and the remaining voxels of the rectum (spheres), and a wire-frame rendering of the 33 Gy iso-dose surface. The 36 Gy iso-dose surface covering the PTV voxel (green) before (b) and after (c) PTV lower bound relaxation. The black arrows indicate where the lower bound for PTV voxels was relaxed, resulting in more voxels not covered by the 36 Gy iso-dose surface. Note that we consider the centroid of the spheres representing the voxels in our constraints.

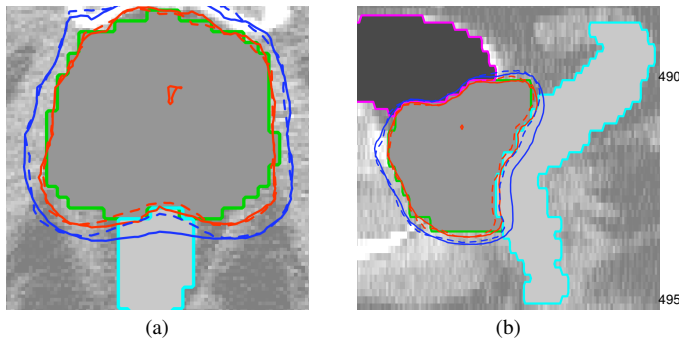


Figure 4 Axial (a) and sagittal (b) slices showing the 33 Gy and 36.25 Gy iso-dose lines before (solid) and after (dotted) all relaxation steps. Changes are limited to the selected region on the rectal wall and to the periphery of the bladder.

### III. RESULTS

#### III.A. Prostate

##### III.A.1. Rectal wall sparing

The initial solution for scenario 1 resulted in a coverage of 99.4 % and a maximum dose to the bladder of 33.0 Gy. To assess the effect of the optimization on a subvolume we considered  $V_\alpha$  as the percentage of the respective VOI receiving a dose of more than  $\alpha$  Gy. Motivated by the potential toxicity of a high rectal wall dose<sup>28</sup>, we selected an area on the rectal wall facing the prostate for further sparing. The selection was done by pushing the surface of the 33 Gy iso-dose away from the rectum and Figure 3a illustrates the actually affected voxels of the rectum as yellow boxes. Running an SSP step to minimize the dose in these voxels only resulted in a 0.1% drop of  $V_{33}$  for the rectum, i.e., no noticeable reduction could be achieved *without* relaxing other bounds.

As a first trade-off we considered relaxing the upper bound on the bladder, but only where the respective upper bound surface was limiting. For small regions on the bladder surface we relaxed the bound from 33.0 to 35.0 Gy. The concurrently running optimizations reduced the  $V_{33}$  of the rectum from 11.1 to 5.5 %, while the maximum dose in the bladder increased only for the selected subvolume of 2.2 %. The dose outside the areas selected for relaxation and the PTV coverage were maintained by constraints and did not deteriorate.

Since the selected area on the rectal wall is very close to

the PTV, relaxing PTV coverage comprised a natural second trade-off. Figure 3b shows the 36 Gy iso-dose surface facing the rectum and covering the PTV almost in its entirety. Figure 3c shows that the 36 Gy iso-dose changed only in a very limited region and only where indicated by the planner. For the related set of PTV voxels the lower bound was reduced to 34.5 Gy, resulting in further drop of the  $V_{33}$  of the rectum to 2.3 % at the expense of a 1.5 % drop in PTV coverage.

The local effect of the trade-offs is highlighted by Figures 4a and 4b, which show that the change in the 33.0 and 36.25 Gy iso-doses is limited to the bladder and PTV regions selected for trade-off while the related improvement in sparing of the selected region in the rectum is also visible. Figure 5 and Table I summarize key statistics on the dose distributions, including the PTV coverage (CO). Note that the optimization times in the table are average values and in case of relaxation mean the automatic optimization when the bounds have been set to the new, relaxed value.

##### III.A.2. Boost volume coverage

Starting with the result of the previous steps we defined a boost volume within one of the prostate lobes for which we defined a target dose of 45.3 Gy, i.e., a dose escalation of 25%. The desired location of the boost volume was determined interactively and an SCO step was performed. While the maximum dose in the PTV increased to 44.25 Gy, none of the selected voxels reached the desired 45.3 Gy. Clearly, PTV voxels around the target area comprised the primarily limiting structure, as they imposed a steep dose fall-off to a maximum dose of 41.5 Gy outside the boost volume. We relaxed the bounds on surrounding areas inside the PTV using the graphical tool, which increased  $V_{45.3}$  to 29.5 %. Furthermore, the visualization indicated that both shell structures around the PTV were limiting. The respective bounds were relaxed in some directions while maintaining a steep gradient towards femoral heads and pelvic bones, resulting in a 12.8 % increase in the coverage of the boost volume. As a further trade-off, additional relaxation along the bladder surface yielded 58.7 % coverage of the boost volume (Fig. 6). Table II summarizes the relaxation steps including the homogeneity index (HI), while Figure III.A.2 shows the DVHs of the initial and resulting dose distributions.

#### III.B. Meningioma

The initial solution for scenario 2 led to 88.7 % coverage, while both OARs received a maximum dose of 7 Gy. Hence the goal was to improve the coverage to the complete PTV (SCO step on all PTV voxels). As a first trade-off we allowed more dose through the nasal and ear cavities by relaxing the outer shell (SHELL2) upper bound in these areas. Figure 7a illustrates limiting areas on the respective iso-dose surface while Figure 7b highlights the voxels selected for relaxation from 4 Gy to 5.5 – 6.0 Gy and the resulting dose fingers. The relaxation allowed for an additional 3.7 % coverage while the dose in the OARs did not change substantially. A similar relaxation of the inner shell (SHELL1) from 10 to 12 Gy lead

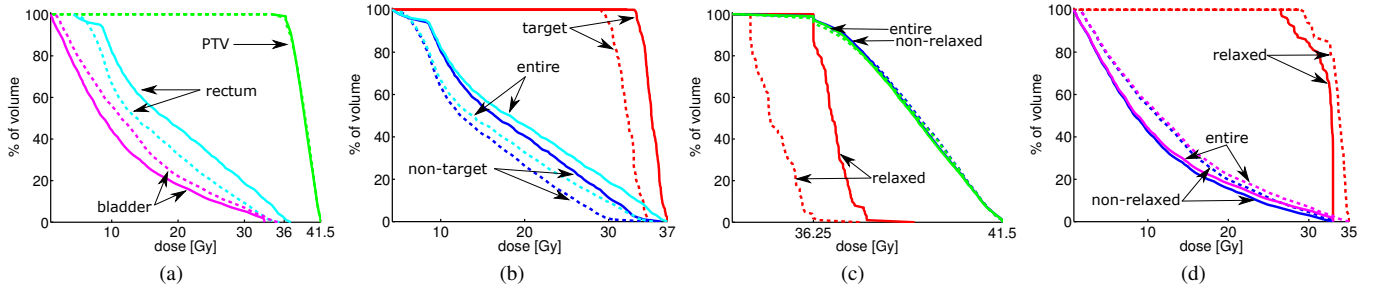


Figure 5 DVHs summarizing the dose distributions for the different VOIs and the respective subvolumes for the initial optimization (solid) and after local PTV and bladder relaxation (dashed), respectively. (a) DVHs for PTV, rectum, and bladder. (b) DVHs for the entire rectum and for its target and non-target subvolumes. (c) DVHs for the entire PTV and for its relaxed and non-relaxed subvolumes. (d) DVHs for the entire bladder and for its relaxed and non-relaxed subvolumes. The DVHs illustrate that only the dose bounds in the selected subvolumes are affected by the relaxation steps.

Table I Summary of the actual dose statistics after local trade-off steps for selective sparing of the rectum. The average runtime is denoted by  $t_{opt}$ . Note that the initial step represents the baseline for interactive planning.

| step          | PTV    |          |          | rectum       |          | bladder      |          | $t_{opt}$ (s) |
|---------------|--------|----------|----------|--------------|----------|--------------|----------|---------------|
|               | CO (%) | min (Gy) | max (Gy) | $V_{33}$ (%) | max (Gy) | $V_{33}$ (%) | max (Gy) |               |
| initial       | 99.4   | 33.99    | 41.50    | 11.2         | 37.00    | 0.0          | 33.00    | -             |
| SSP rectum    | 99.4   | 33.99    | 41.50    | 11.1         | 37.00    | 0.0          | 33.00    | 107           |
| relax bladder | 99.5   | 34.29    | 41.50    | 5.5          | 36.77    | 2.2          | 33.00    | 60            |
| relax PTV     | 98.0   | 34.17    | 41.50    | 2.3          | 35.27    | 2.2          | 35.00    | 61            |

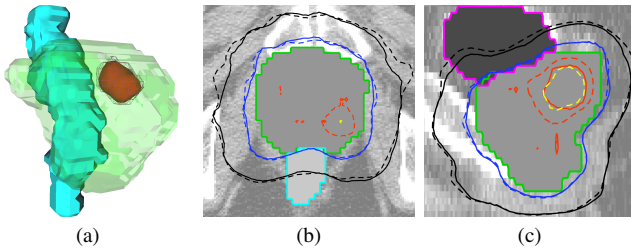


Figure 6 (a) The desired boost volume (wire-frame) and the final 45.3 Gy iso-dose surface. Axial (b) and sagittal slices (c) showing the 20, 33, 41.5 and 45.3 Gy iso-dose lines before (solid) and after (dashed) relaxation. The dashed black contour in the axial slice illustrates the relaxation of the shell towards the sides.

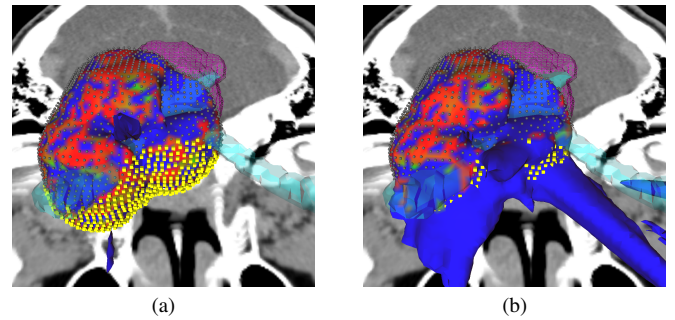
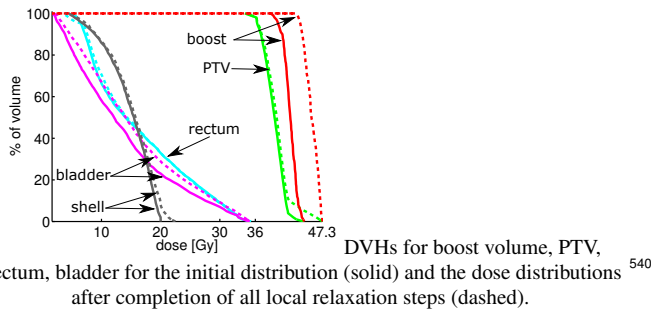


Figure 7 Voxels of SHELL2 represented by spheres where the dose bounds were maintained and by boxes, where the dose bounds were relaxed, and the 4 Gy iso-dose surface: (a) before relaxation SHELL2 contains the iso-dose surface, but some highlighted areas indicate that bounds are limiting the optimization of coverage; (b) after successively relaxing the bounds towards the nasal cavity dose fingers extend in this direction only.



to an additional 0.7 % coverage. Furthermore, the dose constraints implied by optic nerve and brainstem were identified as limiting on the respective bounds surfaces. Therefore, a small region on the surface of the optic nerve was considered for relaxation from 7.0 Gy to 8.0 Gy upper bound. The coverage increased by another 0.3 % while only the selected region of the optic nerve got higher doses. Finally, relaxing the dose along the surface of the brainstem in a similar fashion from 7.0

Gy to 9.0 Gy yielded another 1.2 % increase in PTV coverage. Figure 8 illustrates that the low dose iso-doses only changes in regions that had been relaxed, while the coverage increases for the whole PTV. This is also summarized in Figure 9, which shows that none of the regions that were not relaxed exceeds the original bounds. The results are summarized in Table III, including the conformity index (CI).

#### IV. DISCUSSION

It is important to note that multi-criteria optimization cannot change the physical limits of the dose distribution achievable with a given treatment system. However, it is an effective tool for selecting the dose distribution that represents the best trade-off with respect to the different clinical goals. We have presented an approach that can be used to study how

Table II Summary of the actual dose statistics after steps to increase coverage to the boost volume inside the PTV. The average runtime is denoted by  $t_{opt}$ . Note that the initial step represents the baseline for interactive planning.

| step          | boost  |          | PTV     |      | SHELL1  | SHELL2   | bladder      |          | $t_{opt}$ (s) |
|---------------|--------|----------|---------|------|---------|----------|--------------|----------|---------------|
|               | CO (%) | min (Gy) | max(Gy) | HI   | max(Gy) | max (Gy) | $V_{33}$ (%) | max (Gy) |               |
| initial       | 0.0    | 34.50    | 41.50   | 1.22 | 35.00   | 20.00    | 2.2          | 35.00    | -             |
| SCO boost     | 0.0    | 38.60    | 44.25   | 1.29 | 35.00   | 20.00    | 2.2          | 35.00    | 230           |
| relax PTV     | 29.5   | 39.52    | 47.30   | 1.38 | 35.00   | 20.00    | 2.1          | 35.00    | 24            |
| relax shells  | 42.3   | 41.26    | 47.30   | 1.38 | 37.00   | 22.50    | 2.8          | 35.00    | 12            |
| relax bladder | 58.7   | 42.71    | 47.30   | 1.37 | 37.00   | 22.50    | 4.0          | 35.00    | 117           |

Table III Summary of the actual dose statistics after trade-off steps to improve coverage of the PTV. The average runtime is denoted by  $t_{opt}$ . Note that the initial step represents the baseline for interactive planning.

| step              | PTV    |      |          | optic nerve |          | brainstem |          | $t_{opt}$ (s) |
|-------------------|--------|------|----------|-------------|----------|-----------|----------|---------------|
|                   | CO (%) | CI   | min (Gy) | $V_7$ (%)   | max (Gy) | $V_7$ (%) | max (Gy) |               |
| initial           | 88.7   | 1.08 | 7.80     | 0.0         | 7.00     | 0.0       | 7.00     | -             |
| OCO PTV           | 88.7   | 1.08 | 7.80     | 0.0         | 7.00     | 0.0       | 7.00     | 291           |
| relax SHELL2      | 92.2   | 1.10 | 7.88     | 0.0         | 7.00     | 0.0       | 7.00     | 52            |
| relax SHELL1      | 92.9   | 1.11 | 7.75     | 0.0         | 7.00     | 0.0       | 7.00     | 29            |
| relax optic nerve | 93.2   | 1.12 | 8.23     | 2.8         | 8.00     | 0.0       | 7.00     | 54            |
| relax brainstem   | 94.4   | 1.13 | 8.35     | 2.7         | 8.00     | 0.8       | 8.74     | 47            |

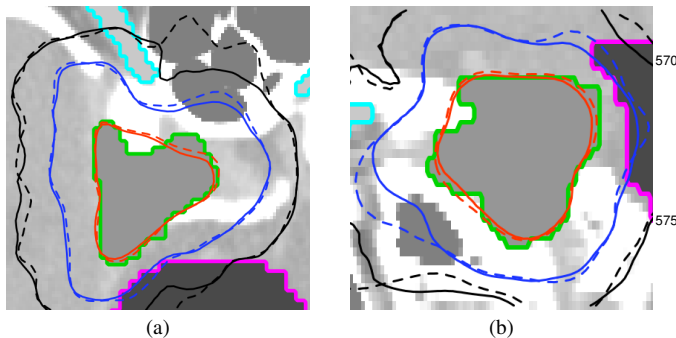


Figure 8 Axial (a) and sagittal (b) slices showing the 4.0 Gy, 7.0 Gy, 10.0 Gy, and 18.0 Gy iso-dose lines before (solid) and after (dashed) all relaxations.

for relaxation, i.e., relaxing at least one binding constraint is a necessary precondition for improvements in the objective and if all binding constraints are relaxed the objective will improve. This illustrates how the method guides the planners search and at the same time depends on the planners decisions: if certain constraints are deemed non-relaxable because the related criteria are crucial the method shows that further progress cannot be expected. This is important information, as it terminates the search.

Relaxation may add more slack than necessary for some voxels, which can be recovered by optimizing the dose of the relaxed voxels towards the previous value. Moreover, relaxation may allow for improvements with respect to other criteria and it is necessary to repeat all optimization steps without relaxation, i.e., in a lexicographic manner, to re-establish Pareto-efficiency. The lexicographic approach is typically considered an a-priori method, i.e., a preference relation among the criteria is defined before starting optimization. However, in our interactive approach we essentially allow the planner to change the preference and restart the process to establish Pareto-efficiency. At the moment this is done after a number of steps and from within the graphical tool and in our experience the effect on the solution is usually small.

We have demonstrated the method in the context of a prostate scenario and a meningioma scenario. While the optimal treatment planning approach for prostate cancer is the subject of ongoing research, stereotactic body radiotherapy and inhomogeneous dose distributions have been considered<sup>21,22,29-31</sup>. Moreover, sparing of the OAR, particularly the rectal wall, is an important goal<sup>28</sup>. Our results illustrate that constraints on the dose distribution which limit local sparing can be identified and systematically relaxed in regions where a trade-off is clinically desirable. We demonstrated that it is possible to selectively spare one region, i.e.,

550 the flexibility of modern treatment devices can be used to spatially shift the dose in the target region. Particularly, the method maintains the dose distribution and highlights spatial constraints, hence allowing for a systematic search for potential trade-offs.

555 Our objective is to shape the dose-distribution, which is defined by the dose in each voxel. Therefore, a single voxel represents the smallest unit of control over the dose distribution and its dose forms a single criterion. Considering the dose of each voxel separately would be possible but often impractical and the graphical tool allows grouping of voxels for SCO, SSP and relaxation. Note that the actual criteria considered remain the doses of the individual voxels, which define the spatial dose distribution. To preserve the dose distribution, each voxel's dose is maintained by a constraint after optimization.

560 While the improvement with respect to the objective is limited by constraints, it is not given that relaxing any specific constraint highlighted in the graphical tool will result in an improvement. However, these constraints present candidates

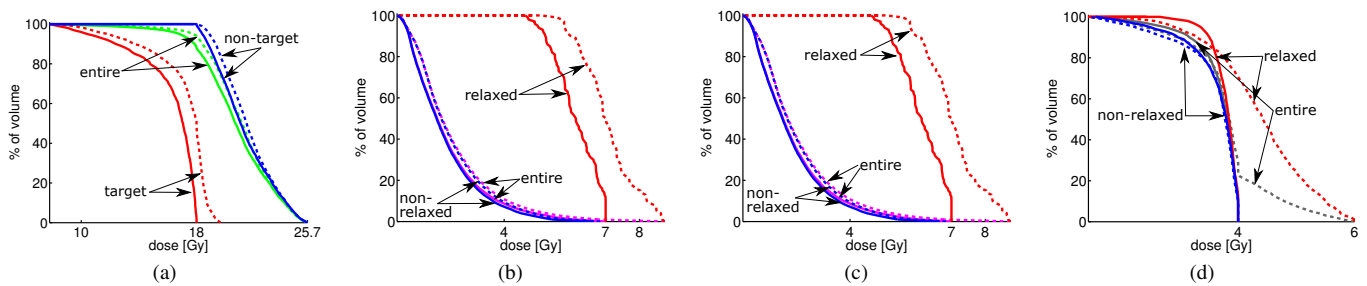


Figure 9 DVHs summarizing the dose distributions for the different VOIs and the respective subvolumes for the initial optimization (solid) and after all relaxations (dashed), respectively. (a) DVHs for the entire PTV and for its target and non-target subvolumes. (b) DVHs for the entire optic nerve and for its relaxed and non-relaxed subvolumes. (c) DVHs for the entire brainstem and for its relaxed and non-relaxed subvolumes. (d) DVHs for the entire SHELL2 and for its relaxed and non-relaxed subvolumes. The DVHs illustrate that only the dose bounds in the selected subvolumes are affected by the relaxation steps.

the dose in the rectal wall was effectively balanced against the dose in a small region on the bladder surface and in the adjacent prostate region. Likewise, we also demonstrated that it is possible to selectively cover a region by studying in which local regions to relax the dose constraints in order to shape a boost volume inside the prostate. A similar trade-off between PTV coverage and OAR sparing is typical for planning treatments close to the optic nerves<sup>24,25</sup>, where the planner is frequently willing to compromise coverage locally, but not globally. Again, we illustrated for scenario 2 that the dose distribution can be locally modified based on information where constraints limit progress and an assessment of whether relaxing these constraints is clinically acceptable.

Conventionally, the dose distribution is considered by studying DVHs. The main limitation of this approach is the neglect of spatial information. Recently, more complex spatial dose distributions have been studied in the context of dose painting. Typically, the objective function for treatment plan optimization defines different target doses for specific regions or individual voxels for dose-painting by contours (DPBC)<sup>32,33</sup> and dose-painting by numbers (DPBN)<sup>20,34–36</sup>, respectively. However, this does not solve the inherent conflict among the related goals and the resulting dose-distribution will typically not fulfill all goals simultaneously. Obviously, changing the importance of certain regions, e.g., by increasing the respective coefficients in the objective function or by modifying the desired dose, will change the dose distribution<sup>2,3</sup>. Generally, these changes implicitly affect the global dose distribution, e.g., it has been reported that a higher boost in one region comes at the cost of less dose increase in other regions<sup>32</sup>.

In contrast, our method allows to maintain the dose distribution. Conceptually, it is closer to DPBC, although we do not consider contours explicitly. Instead, the possibility to shape the iso-dose-surfaces is studied, i.e., there is no need to define a set of auxiliary structures. This also extends current multi-criteria approaches, which typically consider criteria on a VOI level. In fact, considering a large number of fine grained dose criteria would be a challenge for methods that compute the Pareto-frontier upfront and would have to deal with a large search space. Our hypothesis is that starting from a reasonable dose distribution the human planner will be able to identify where the iso-dose surface needs to be shaped, i.e.,

solutions which prioritize other criteria will not be explored. Clearly, the interactive approach we propose depends on a fast optimization, which is currently below 1 minute for typical relaxation steps.

## V. CONCLUSION

The presented approach allows to systematically explore trade-offs with respect to the spatial dose distribution. Starting from an initial dose distribution a graphical tool allows to locally modify the shape of one iso-dose surface. The desired modification is mapped to either of two optimization steps: selective coverage and selective sparing. Constraints maintain the dose distribution everywhere else. Regions where these constraints limit the optimization are visualized to the planner and can be explicitly relaxed to realize the trade-off. The examples illustrate that the method can be used to fine-tune the balance between OAR sparing and PTV coverage.

## REFERENCES

- L. Xing, J. G. Li, S. Donaldson, Q. T. Le, and A. L. Boyer, "Optimization of importance factors in inverse planning," *Phys. Med. Biol.* **44**, 2525–2536 (1999).
- C. Cotrutz and L. Xing, "Imrt dose shaping with regionally variable penalty scheme," *Med Phys* **30**, 544–551 (2003).
- P. Lougovski, J. LeNoach, L. Zhu, Y. Ma, Y. Censor, and L. Xing, "Toward truly optimal IMRT dose distribution: Inverse planning with voxel-specific penalty," *Technology in cancer research & treatment* **9**, 629–636 (2010), PMID: 21070085 PMCID: PMC3057528.
- Y. Yu, "Multiobjective decision theory for computational optimization in radiation therapy," *Med. Phys.* **24**, 1445–1454 (1997).
- H. W. Hamacher and K.-H. Küfer, "Radiation therapy planning - a multi-criteria linear programming problem," *Discrete Applied Mathematics* **118**, 145–161 (2002).
- M. Lahanas, E. Schreibmann, and D. Baltas, "Multiobjective inverse planning for intensity modulated radiotherapy with constraint-free gradient-based optimization algorithms," *Phys. Med. Biol.* , 2843–2871 (2003).
- H. Romeijn, J. Dempsey, and J. Li, "A unifying framework for multi-criteria fluence map optimization models," *Phys. Med. Biol.* **49**, 1991–2013 (2004).
- E. Schreibmann, M. Lahanas, L. Xing, and D. Baltas, "Multiobjective evolutionary optimization of the number of beams, their orientations and weights for intensity-modulated radiation therapy," *Phys. Med. Biol.* **49**, 747–770 (2004).
- I. Rosen, H. H. Liu, N. Childress, and Z. Liao, "Interactively exploring optimized treatment plans," *Int. J. Radiation Oncology Biol. Phys.* **61** (2005).

- <sup>10</sup>D. Craft, T. Halabi, and T. Bortfeld, "Exploration of tradeoffs in intensity-modulated radiotherapy," *Phys. Med. Biol.* **50**, 5857–5868 (2005), PMID: 16333160.
- <sup>11</sup>M. Monz, K. H. Küfer, T. R. Bortfeld, and C. Thieke, "Pareto navigation: algorithmic foundation of interactive multi-criteria imrt planning," *Phys. Med. Biol.* **53**, 985–998 (2008).
- <sup>12</sup>J. I. Serna, M. Monz, K. H. Küfer, and C. Thieke, "Trade-off bounds for the pareto surface approximation in multi-criteria imrt planning," *Phys. Med. Biol.* **54**, 6299–6311 (2009).
- <sup>13</sup>K.-W. Jee, D. L. McShan, and B. A. Fraass, "Lexicographic ordering: intuitive multicriteria optimization for IMRT," *Phys. Med. Biol.* **52**, 1845–1861 (2007).
- <sup>14</sup>J. J. Wilkens, J. R. Alaly, K. Zakarian, W. L. Thorstad, and J. O. Deasy, "IMRT treatment planning based on prioritizing prescription goals," *Phys. Med. Biol.* **52**, 1675–1692 (2007).
- <sup>15</sup>A. Schlaefler, O. Blanck, and A. Schweikard, "Interactive multi-criteria inverse planning for robotic radiosurgery," in *Proceedings of the XVth International Conference on the Use of Computers in Radiation Therapy (ICCR)*. (2007).
- <sup>16</sup>A. Schlaefler and A. Schweikard, "Stepwise multi-criteria optimization for robotic radiosurgery," *Med. Phys.* **35**, 2094–2103 (2008), PMID: 18561685.
- <sup>17</sup>A. Schlaefler and O. Blanck, "TU-EE-A1-05: exploring the spatial trade-off in treatment planning," *Med. Phys.* **35**, 2910 (2008).
- <sup>18</sup>T. Viulet, N. Rzevovski, and A. Schlaefler, "SU-C-BRC-03: three-dimensional isodose surface manipulation for multi-criteria inverse planning in radiosurgery," (AAPM, 2011) pp. 3371–3371.
- <sup>19</sup>Viulet, T, Rzevovski, N, and Schlaefler, A, "Towards interactive planning for radiotherapy by three-dimensional iso-dose manipulation," in *International Journal of Computer Assisted Radiology and Surgery*, Vol. 6 (Springer, Berlin, Germany, 2011) p. S57.
- <sup>20</sup>S. M. Bentzen, "Dose painting and theragnostic imaging: towards the prescription, planning and delivery of biologically targeted dose distributions in external beam radiation oncology," *Cancer Treat Res* **139**, 41–62 (2008).
- <sup>21</sup>T. Dirscherl, M. Rickhey, and L. Bogner, "Feasibility of TCP-based dose painting by numbers applied to a prostate case with (18)f-choline PET imaging," *Z Med Phys* **22**, 48–57 (2012).
- <sup>22</sup>J. H. Chang, D. Lim Joon, S. T. Lee, S. J. Gong, N. J. Anderson, A. M. Scott, I. D. Davis, D. Clouston, D. Bolton, C. S. Hamilton, and V. Khoo, "Intensity modulated radiation therapy dose painting for localized prostate cancer using c-choline positron emission tomography scans," *Int J Radiat Oncol Biol Phys* **83**, e691–e696 (2012).
- <sup>23</sup>S. E. Combs, D. Schulz-Ertner, D. Moschos, C. Thilmann, P. E. Huber, and J. Debus, "Fractionated stereotactic radiotherapy of optic pathway gliomas: tolerance and long-term outcome." *Int J Radiat Oncol Biol Phys* **62**, 814–819 (2005).
- <sup>24</sup>P. Romanelli, L. Bianchi, A. Muacevic, and G. Beltramo, "Staged image guided robotic radiosurgery for optic nerve sheath meningiomas," *Comput Aided Surg* **16**, 257–266 (2011).
- <sup>25</sup>K. C. Cuneo, T. M. Zagar, D. M. Brizel, D. S. Yoo, J. K. Hoang, Z. Chang, Z. Wang, F. F. Yin, S. K. Das, S. Green, N. Ready, M. T. Bhatti, D. M. Kaylie, A. Becker, J. H. Sampson, and J. P. Kirkpatrick, "Stereotactic radiotherapy for malignancies involving the trigeminal and facial nerves," *Technol Cancer Res Treat* **11**, 221–228 (2012).
- <sup>26</sup>C. King, "Stereotactic body radiotherapy for prostate cancer: current results of a phase ii trial." *Front Radiat Ther Oncol* **43**, 428–437 (2011).
- <sup>27</sup>A. Schweikard, A. Schlaefler, and J. R. Adler, "Resampling: An optimization method for inverse planning in robotic radiosurgery," *Med. Phys.* **33**, 4005–4011 (2006).
- <sup>28</sup>O. Acosta, G. Drean, J. D. Ospina, A. Simon, P. Haigrón, C. Lafond, and R. de Crevoisier, "Voxel-based population analysis for correlating local dose and rectal toxicity in prostate cancer radiotherapy," *Phys Med Biol* **58**, 2581–2595 (2013).
- <sup>29</sup>D. B. Fuller, J. Naitoh, C. Lee, S. Hardy, and H. Jin, "Virtual HDr cyberknife treatment for localized prostatic carcinoma: dosimetry comparison with HDr brachytherapy and preliminary clinical observations." *Int J Radiat Oncol Biol Phys* **70**, 1588–1597 (2008).
- <sup>30</sup>D. E. Freeman and C. R. King, "Stereotactic body radiotherapy for low-risk prostate cancer: five-year outcomes," *Radiation Oncology* **6**, 3 (2011).
- <sup>31</sup>C. R. King, J. D. Brooks, H. Gill, and J. C. Presti, Jr, "Long-term outcomes from a prospective trial of stereotactic body radiotherapy for low-risk prostate cancer." *Int J Radiat Oncol Biol Phys* **82**, 877–882 (2012).
- <sup>32</sup>G. Meijer, J. Steenhuijsen, M. Bal, K. De Jaeger, D. Schuring, and J. Theuws, "Dose painting by contours versus dose painting by numbers for stage ii/iii lung cancer: practical implications of using a broad or sharp brush." *Radiother Oncol* **100**, 396–401 (2011).
- <sup>33</sup>D. Thorwarth and M. Alber, "Implementation of hypoxia imaging into treatment planning and delivery," *Radiother Oncol* **97**, 172–175 (2010).
- <sup>34</sup>E. T. Bender, "Using spatial information about recurrence risk for robust optimization of dose-painting prescription functions." *Med Phys* **39**, 2713–2720 (2012).
- <sup>35</sup>S. M. Bentzen and V. Gregoire, "Molecular imaging-based dose painting: a novel paradigm for radiation therapy prescription." *Semin Radiat Oncol* **21**, 101–110 (2011).
- <sup>36</sup>Y. Kim and W. A. Tom, "Dose-painting imrt optimization using biological parameters." *Acta Oncol* **49**, 1374–1384 (2010).